A Procedure for Fitting Point Sources in SMEI White-Light Full-Sky Maps.

P. Hick, A. Buffington and B.V. Jackson

Center for Astrophysics and Space Sciences, University of California San Diego

ABSTRACT

The Solar Mass Ejection Imager (SMEI) instrument consists of three CCD cameras with individual fields of view of 60°×3° that combined sweep a 160° arc of sky. SMEI covers the entire sky in one spacecraft orbit of 102 minutes. Individual 4-s exposures from each orbit are assembled into full-sky maps. The primary objective in the SMEI data reduction is to isolate the Thomson-scattering signal across the sky from free electrons in the solar wind. One of the steps needed to achieve the required photometric precision is the individual fitting and removal of stars brighter than 6^{th} magnitude from the full-sky maps. The point-spread function of the SMEI optics has several unusual properties. It has a full width of about one degree, is asymmetric, and varies in width depending on where in the field of view the image is formed. Moreover, the orientation of the PSF on the sidereal sky rotates over 360° over the course of a year. We describe the procedure used to fit and subtract individual stars from the SMEI full-sky maps. A by-product of this procedure are time series at the orbital time resolution for stars brighter than 6^{th} magnitude. These results are used by Buffington *et al.* (2007)[1] to calibrate the SMEI instrument against the LASCO C3 coronagraph.

Keywords: Solar Mass Ejection Imager, data processing, full-sky maps, point spread function, least squares fit

1. INTRODUCTION

The Solar Mass Ejection Imager[2,3] is a full-sky, white-light, CCD-based camera system for observing the inner heliosphere from Earth orbit. SMEI was launched into an 840 km Sun-synchronous terminator orbit on January 6, 2003. It shares the Air Force Coriolis Mission spacecraft with the U.S. Navy WindSat instrument. Several sources contribute to the total signal seen by SMEI: light from planets, stars and galaxies, scattered sunlight from the zodiacal dust cloud[4], Thomson-scattered sunlight from free electrons in the solar wind, and, especially during times of high geomagnetic activity, auroral light[5]. The primary science objective of SMEI is the study of solar wind structures (such as coronal mass ejections and corotating structures) in the inner heliosphere by measuring the Thomson-scattering brightness from these structures. To isolate the Thomson scattering signal all other sources of white light in the data need to be removed[6]. This paper focuses on the procedure used to remove point sources, *i.e.* bright stars and planets.

SMEI consists of three cameras, each with a field of view of roughly 60°×3°, aligned in such a way on the spacecraft that combined they image a strip of sky of about 160°×3°. As the spacecraft moves through its polar orbit, the SMEI cameras continuously take 4-second exposures and sweep nearly the entire sky over each 102-minute orbit. CCD frames from each orbit (typically 1500 from each camera) are combined to provide a photometric white-light map of the sky as visible from Earth orbit. Point sources are removed from these composite skymaps, rather than from the individual CCD frames. A typical sky location transits the field of view at an approximately fixed position in the long dimension of the field of view, crossing the 3° narrow dimension in about one minute. Thus, about a dozen or more sequential CCD frames contribute to the brightness at that location in the composite skymap.

The point spread function (PSF) of the SMEI cameras has a highly asymmetric fish-like shape [6,7]resulting from comatic and spherical aberration, and varies in shape with position in the field of view both in the narrow

P.H.: E-mail: pphick@ucsd.edu, Tel. (858) 534-8965;
A.B.: E-mail: abuffington@ucsd.edu, Tel. (858) 534-6630;
B.V.J.: E-mail: bvjackson@ucsd.edu, Tel. (858) 534-3358

Solar Physics and Space Weather Instrumentation II, edited by Silvano Fineschi, Rodney A. Viereck
Proc. of SPIE Vol. 6689, 66890C, (2007) · 0277-786X/07/$18 · doi: 10.1117/12.734808

and long dimension[1] of each camera. For a given point source the effective PSF in the composite skymaps is a net average resulting from superposition of all contributing CCD frames. This procedure averages the variation of the CCD PSF with position along the narrow dimension. The variation with position along the long dimension (primarily a change in the width of the PSF) remains noticeable in the effective skymap PSF.

In order not to compromise the photometric specification for SMEI (0.1% differential photometry per square degree of sky) point sources brighter than 6^{th} magnitude are removed individually from the composite skymaps. A star catalogue (with magnitudes and positions in J2000 equatorial coordinates) was constructed prior to launch from available catalogues, taking into account the SMEI bandpass to estimate the brightness of these stars. The resulting list of approximately 5600 stars is used as the primary list of sources to be removed from the skymaps, augmented with the brightest planets (Jupiter, Saturn, Venus and Mars). Planetary positions are determined using the DE405 planetary ephemeris of Dr. E.M. Standish (NASA/JPL).

2. THE SMEI FULL-SKY POINT SPREAD FUNCTION (PSF)

The SMEI full-sky maps are assembled and stored as three different maps, together covering the entire sky (with some overlap between the maps) using the J2000 equatorial reference frame. An equatorial map covers the sky between declinations -60° and +60° using an equirectangular projection with the equator as the standard parallel. The angular resolution is 0.1° (this map has 3600×1200 bins). The north and south polar regions above 50° in absolute declination are covered using a polar projection with a 0.1° resolution in declination (these maps have 800×800 bins). The shape and size of a bright star in these composite skymaps is influenced by three factors. First, the star is an average of contributions from a dozen or more sequential CCD frames where the star crossed the field of view at an angle $|\theta|$ less than 30° from the optical axis of the camera. The width of star PSF varies as $\cos\theta$. Second, since the orbital plane of the sun-synchronous orbit rotates 360° over the course of one year, the star PSF accordingly changes its rotates around its centroid in the skymap. Thirdly, the map projection distorts the star PSF depending on the location of the star in the skymap.

To establish a reference PSF or "standard star" for use in the fitting procedure for bright stars, a group of isolated stars (with no close neighbouring stars) was selected: Aldebaran (α Tau), Betelgeuse (α Ori), Sirius (HD 48915), Vega (α Lyr), Alkaid (HD 120315), Eta Draconis, Almach (HD 12533), HD 20902, NSV 6846, HD 124897, HD 164058 and HD 123139. For a selection of skymaps throughout a period of one year these stars were superposed and averaged after subtracting a suitable background and correcting for the three effects mentioned in the previous paragraph. The resulting, empirically determined, PSF or "standard star" is shown in Figure 1 for each of the three SMEI cameras.

2.1. Orientation of the PSF on the sky

The orbital plane of the Coriolis spacecraft maintains an approximately fixed orientation relative to the Sun-Earth line, resulting in a full 360° rotation relative to the sidereal sky over the course of one year. As a result the orientation of the fields of view of the three cameras, and hence the PSF, changes its orientation relative to the sidereal sky. Near the poles the change is a near-uniform rotation; away from the poles it becomes increasingly non-uniform. Figure 2 shows the same part of the sky near Orion at two different times, on November 10, 2005 and January 19, 2006 (about two months later), illustrating this change of orientation of the PSF. The expected orientation of the PSF for every star can be calculating from known spacecraft attitude information and the location of star, and is described as the angle between the symmetry axis of the PSF (the "up" direction in Figure 1) and equatorial north. The closest star to either north or south pole in the SMEI star catalogue is Polaris (HD 8890) at 44 arcmin away from the north pole. This is still far enough away from the pole to avoid problems with this definition for the PSF orientation.

2.2. Width of the PSF

The width of the PSF on a CCD frame decreases proportional to $\cos\theta$ as the position is further away from the optical axis of the camera in the long dimension of the field of view. Only the width perpendicular to the PSF symmetry axis (in the θ direction) is affected. In the SMEI skymaps this results in a more narrow PSF if the star is constructed from portions of CCD frames far removed from the optical axis. The method of assembling the skymap ensures that the integrated intensity in the star (after the background is subtracted) stays the same (*i.e.*,

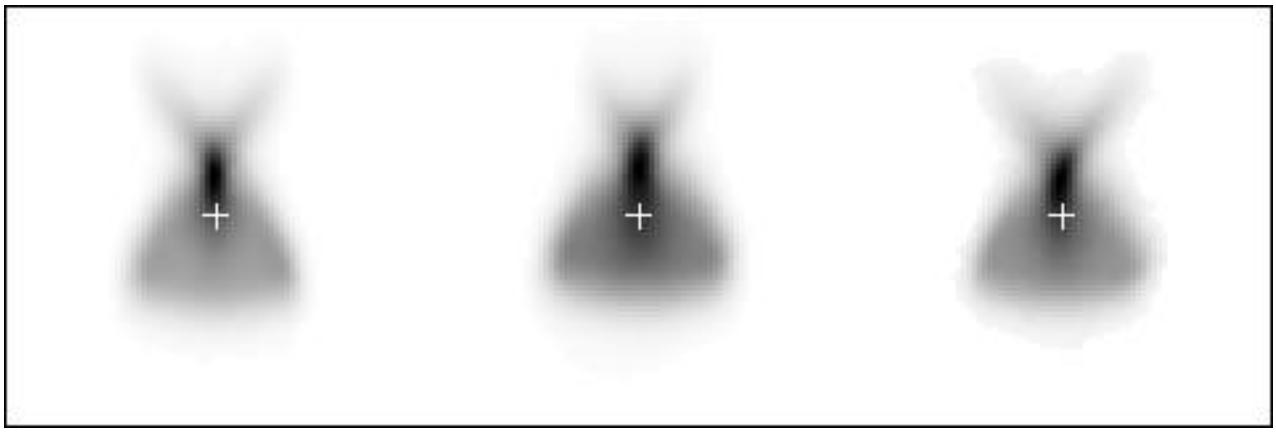

Figure 1. The "standard stars" for SMEI cameras 1, 2 and 3 (left to right) shown in the same equirectangular projection as used for the equatorial skymaps. The crosses indicate the location of the centroid ("center of mass") of the brightness distribution. The standard star is constructed with an angular resolution of 0.025°. For each camera a 2°×2° square is shown. The standard star can be viewed as a star with its centroid located in the equatorial skymap at the vernal equinox (α=0, δ=0) with the axis of symmetry in the equatorial north-south direction (north is up) and composed from a sequence of CCD frames in which the star transits the field of view near the optical axis (at $\theta = 0$). The effective non-zero area of this PSF is 1.18 square degrees for camera 1, 1.32 for camera 2 and 1.05 for camera 3.

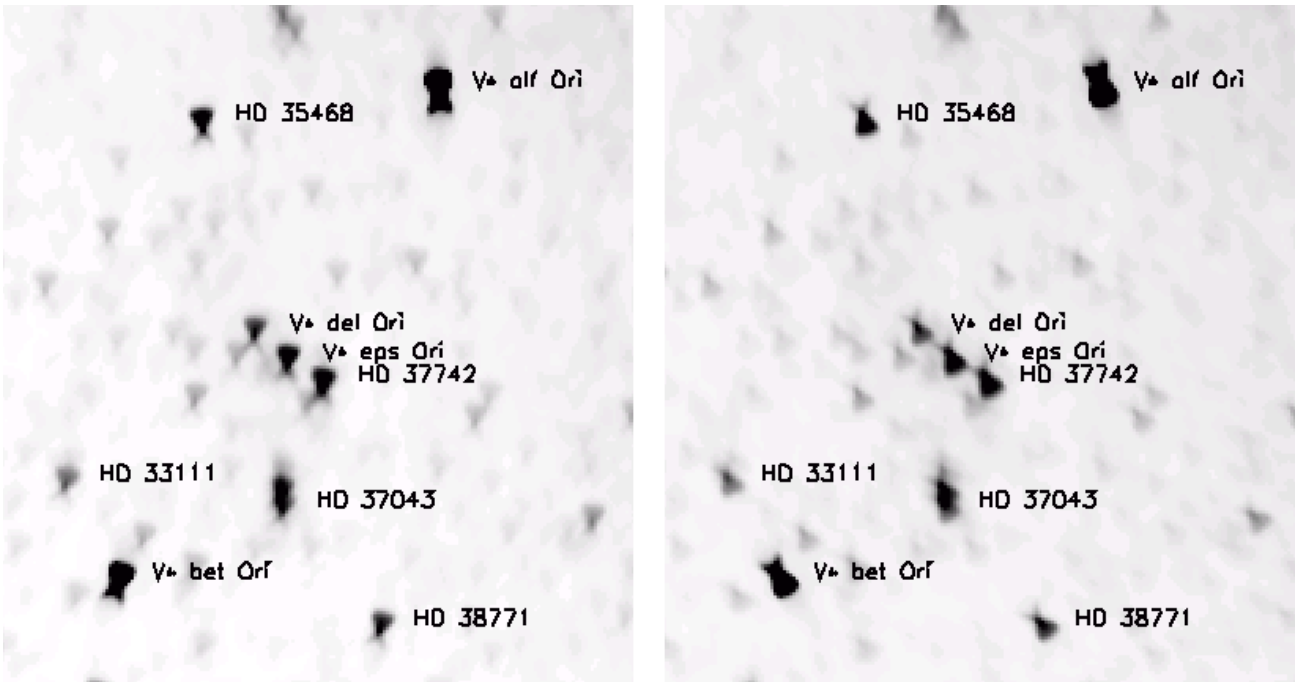

Figure 2. The constellation of Orion, extracted from SMEI full-sky maps. Left: in SMEI orbit 14800 (starting at 2005/11/10 03:24:54 UT). Right: in SMEI orbit 15800 (starting at 2006/01/19 16:37:21 UT). The different orientation of the asymmetric PSF results from the rotation of the spacecraft orbit relative to the sidereal background. In both orbits Orion is viewed by SMEI camera 1 (pointing away from the Sun). The greyscale is set to saturate at 1000 ADU (analog-to-digital units[1]). Of the labeled stars only HD 33111 and δ Ori are not saturated. The brightest star, α Ori, peaks at about 21000 ADU. The map covers the area 75° $<\alpha<$95°, -13°$<\delta<$11° (right ascension increases left to right).

is independent of θ). Let $f_{std}(x,y)$ be the brightness distribution in the standard star of Figure 1 (with θ=0). x and y are coordinates perpendicular to and along the symmetry axis, respectively. The origin ($x=0$,$y=0$) is at the centroid of the PSF (x and y effectively are the right ascension and declination across the PSF with the centroid at $\alpha=0$, $\delta=0$). Let $f(x,y)$ be the brightness distribution of a test star differing only from the standard star by having $|\theta|>0$. The integrated brightness in the standard and the test star then are:

$$\begin{aligned} B_{std} &= \int_{L_{1,x}}^{L_{2,x}} dx \int_{L_{1,y}}^{L_{2,y}} dy\, f_{std}(x,y) \\ B &= \int_{L_{1,x}\cos\theta}^{L_{2,x}\cos\theta} dx \int_{L_{1,y}}^{L_{2,y}} dy\, f(x,y) \end{aligned} \tag{1}$$

$L_{1,x}$, $L_{2,x}$, $L_{1,y}$, $L_{2,y}$ indicate the ranges in x and y over which the standard PSF is non-zero. The factor $x\cos\theta$ in the integration limits for the test star brightness B reflects the shrinking of the PSF width in the x-direction with increasing $|\theta|$. The simplest way to satisfy the requirement $B=B_{std}$ is to assume:

$$f(x,y) = \frac{1}{\cos\theta} f_{std}\left(\frac{x}{\cos\theta}, y\right) \tag{2}$$

3. LEAST-SQUARES FIT OF A SINGLE POINT SOURCE

A box of 5°×5° (50×50 bins) is selected from a skymap centered on the location of a bright star as given in the SMEI star catalogue. For all pixels in this box the location and sky brightness are known. Then

$$F(r_{ij}) = F_{ij} \quad (i\in[1,N],\ j\in[1,M] \tag{3}$$

where the position is specified in terms of array indices (i,j) into the skymap array:

$$r_{ij} = (i,j)\ \ i\in[1,N];\ j\in[1,M] \tag{4}$$

In this box the star centroid is located near $i_s=\frac{1}{2}(N+1)$, $j_s=\frac{1}{2}(M+1)$. For the equatorial map $N=3600$, $M=1200$; for the polar maps $N=M=800$. In its simplest form a star is fitted using a template that consists of a planar sloped background and a "standard star" with a scaling factor:

$$F(r_{ij}) = A + a(i-i_s) + b(j-j_s) + B\,F^{std}(\overline{r}_{ij}) \tag{5}$$

where $F^{std}(\overline{r}_{ij})$ are the brightnesses in the standard star at the equivalent locations $\overline{r}_{ij}$. The equivalent locations $\overline{r}_{ij}$ are obtained from r_{ij} by applying a sequence of transformations:

- convert from bin location r_{ij} in the skymap to J2000 equatorial coordinatees. This amounts to applying the inverse of the map projection, *ProjMap*. For the equirectangular equatorial map this is a simple linear scaling; for the polar maps it is the inverse of a polar transformation.
- apply a rotation *RotatePSF* to account for the PSF orientation on the sky.
- apply a rotation *RotatePos* to convert from equatorial coordinates near the star centroid to equatorial coordinates near the standard star centroid (at the vernal equinox, $\alpha=\delta=0$).
- apply a scaling factor $\cos^{-1}\theta$ to the right ascension only (it is assumed that the right ascension is in the range $-\pi<\alpha<\pi$). Call this operation *Stretch*. This accounts for the variation of the PSF width with angle θ (Section 2.2).
- convert from equatorial coordinates to array indices in the "standard star" array. This amounts to applying the equirectangular map projection, *ProjStd*, used for the "standard star" map. This is a linear scaling in both dimensions.

This can be summarized symbolically by:

$$\overline{r}_{ij} = \left(ProjStd \times Stretch \times RotatePos \times RotatePSF \times ProjMap^{-1}\right) r_{ij} \tag{6}$$

The standard star brightnesses $F^{std}\left(\overline{r}_{ij}\right)$ are obtained by linear interpolation in the "standard star" map at the equivalent locations, and are then multiplied by $\cos^{-1}\theta$ to ensure that the integrated intensity of the star is preserved (Eq. 2). In the linear fit each skybin is assigned a weight inversely proportional to the intensity in the full-sky map. This is especially important when fitting bright stars to obtain an accurate fit of the brightness in the background.

Eq. 5 is fitted to the bright star using a linear least-squares fit in three dimensions. The constants A, a, b provide the background at the location of the bright star in the map; the constant B provides the ratio of the brightness of the star to that of the "standard star". The area around the star used in the least-square fit includes all skybins that map to equivalent locations inside the effective area of the PSF (Figure 1 and an additional area extending out to a radius of typically 1.4° from the star centroid. This latter area ensures that enough skybins are used to fit the background by including bins that are safely away from the PSF itself.

4. STAR CROWDING

Stars are fit and removed from the skymap in order of increasing magnitude (decreasing brightness). This is done to minimize the impact of nearby brighter stars on the quality of the fit. However, in cases where stars brighter than 6^{th} magnitude lie very close together (less than the width of the PSF, Figure 1) this is not sufficient, and it becomes necessary to include multiple stars in a single fit. Currently stars are fitted simultaneously if their catalogue positions are closer together than 0.75°. An additional complication is that occasionally a star will have a close neighbour at a distance substantially less than the width of the PSF. In these cases these stars cannot be separated anymore. Currently if stars are closer than 0.25° the brighter star is fit first and is assumed to include the brightness of the fainter star. The fainter star is not fit at all.

The above procedure is extended to include more than one star. The template in Eq. 5 is generalized to:

$$F(r_{ij}) = A + a\,(i - i_s) + b\,(j - j_s) + \sum_k B_k\, F^{std}\left(\overline{r}^k_{ij}\right) \tag{7}$$

where the summation is over all the stars that need to be fitted simultaneously. (i_s, j_s) usually refers to the location of the brightest star in the group. Note that the equivalent positions for each of the stars $\overline{r}^k_{ij}$ depend on the location of the star (primarily through the rotation operator *RotatePos* in Eq. 6). The least-squares fit of Eq. 7 again is a linear fit, this time in $k + 2$ dimensions. We currently fit up to four stars simultaneously (a bright star with up to three close and fainter neighbours), resulting in a linear fit over six dimensions.

5. ADDITIONAL CONSIDERATIONS FOR FITTING POINT SOURCES

The least-squares fit described above has the advantage that it is computationally efficient. For instance, removal of all 5600 stars in the SMEI catalogue from a full-sky map takes a few minutes on a PC with a 3 GHz CPU. However, there are several reasons why it would be desirable to extend the fit. The most obvious is that a star centroid in the skymap is not at the exact catalogue location, either because the catalogue position is wrong, or because the spacecraft attitude was slightly wrong (and the star was "dropped" into the skymap at the wrong location). Thus, one would like to include the centroid locations as free parameters in the fit. The angle defining the orientation of the PSF on the sky relative to equatorial north (Section 2.1) also is derived from the (sometimes slightly wrong) spacecraft attitude information, and hence ideally is included in the fit too.

The PSF on the CCD varies in a somewhat complicated way as a function of position across the field of view, as reflected for instance in the variation of the width of the PSF width angular distance from the optical axis (Section 2.2). The full-sky PSF shown in Figure 1 was derived empirically from the skymaps themselves. In the skymaps (and hence the sky PSF) the variation width location along the narrow dimension is effectively averaged away because in general stars travel across the field of view in that direction. However, this is only approximately true, especially near the anti-solar edge of camera 1, where stars travel a substantial distance

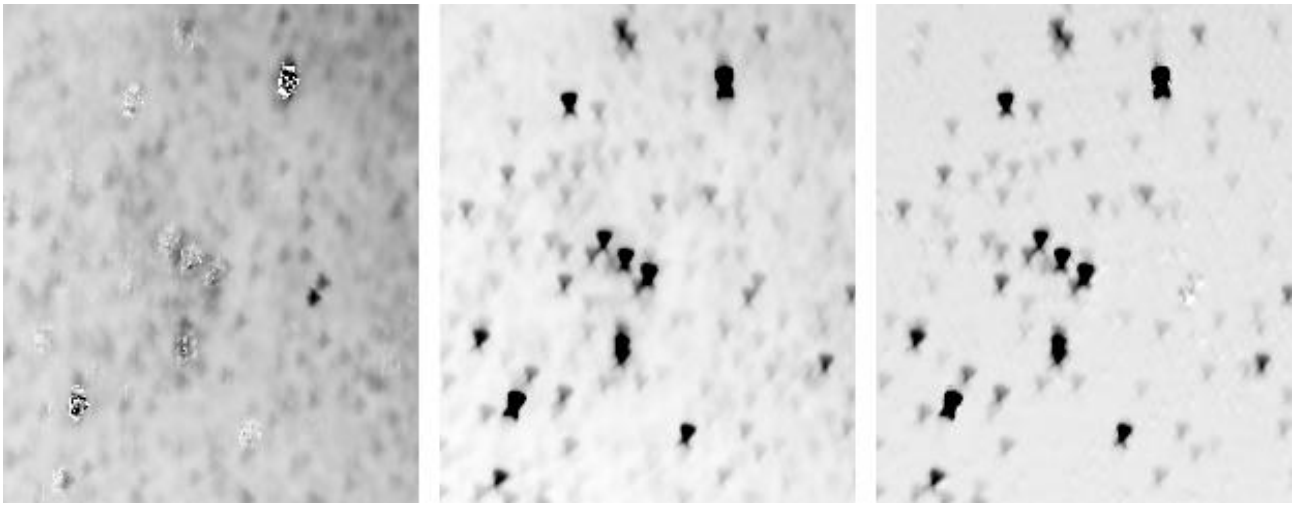

Figure 3. Orion in SMEI skymaps for orbit 14800. Left: the unresolved sidereal background. The average brightness in the background over this section of sky is 62 ADUs . Center: the skymap with the average background brightness taken away. Right: the skymap with the actual background map (left) taken away. The greyscale for the skymaps covers the range 0 to 500 ADUs. from white to black The scale for the background map (left) is enhanced by a factor of three (*i.e.*, covers the range 0 to 500/3 ADUs).

along the long dimension while crossing the field of view. A further complication is that SMEI CCD frames are available in "engineering mode" (at the full resolution of the CCD) and in "science mode" (2×2 binned for camera 3, 4×4 binned for cameras 1 and 2). The sky PSF was determined from skymaps constructed from engineering mode frames. However, the bulk of the skymaps are constructed from science mode frames. The effect of the binning on the sky PSF is not taken into account and is currently considered as one possible cause for small differences in star brightnesses determined from skymaps constructed from engineering mode data versus science mode data. Thus, the sky PSF from Figure 1 represents a good average representation of the PSF across the sky, but small deviations are still expected to be present. One obvious way to account for small variations in the PSF is to allow the width of the PSF to vary, both along the symmetry axis and perpendicular (in addition to the $\cos\theta$ dependence) as free parameters in the least squares fit.

These five additional parameters (centroid coordinates, PSF orientation angle, and the PSF widths) are not easily included in an analytic least-square procedures, but have been implemented as free parameters using a brute force approach that iteratively steps through a five-dimensional parameter space until a best fit is found. This procedure is currently computationally too slow to be practical for the whole SMEI skymap data base, and is only expected to be useful for limited stretches of data.

6. UNRESOLVED SIDEREAL BACKGROUND

Prior to fitting and subtracting individual stars the unresolved sidereal background (primarily the galactic background, and including stars fainter than 6^{th} magnitude) is subtracted. This background map is determined empirically from engineering mode data from SMEI camera 2. A map covering the entire sky constructed from engineering mode data taken throughout a whole year is separated into individual bright stars, zodiacal dust cloud and diffuse galactic background. The galactic background map is used for all three cameras, taking into account the differing gains of the cameras (the gain of camera 1 is 0.97 as compared to camera 2; the gain for camera 3 is 0.92 that of camera 2), and the decrease of the gain with time of 1.6% per year. The subtraction of the sidereal background for Orion is illustrated in Figure 3. The main motivation for subtracting the diffuse sidereal background prior to subtracting individual bright stars is to reduce higher-order derivatives in the underlying background brightness distribution, making it more consistent with the assumption of a planar background in the template used for the star subtraction (Eq. 5).

7. RESULTS OF POINT SOURCE SUBTRACTION

The section of sky in the constellation Orion shown in Figure 2 contains 149 stars listed in the SMEI star catalogue. Figure 4 shows results for star subtraction in this area using two methods: the basic analytic least squares fit described in Sections 3 and 4, and a least squares fit with iterative solutions for centroid, PSF width and PSF orientation. For comparison, when run on a PC with a 600 MHz CPU the running times are 2.5 minutes and 6 hours, respectively, for this section of sky.

The iterative fitting does substantially improve the quality of the fit, especially for bright stars. For the five brighest stars in Orion the standard deviation of the residual intensity after subtracting the stars decreases: αOri from 464 to 245 ADU; β Ori from 196 to 124 ADU; HD 35468 from 40 to 33 ADU; HD 37742 from 118 to 69 ADU; εOri from 102 to 67 ADU. A visual inspection of the top two maps in Figure 4 confirms this. For instance, the three stars in Orions belt are removed more effectively. However, the residual brightnesses after a very bright star has been removed can still be significant, in part because of the inherent noise in the star, but also because of apparent deficiencies in the PSF shape (as evidenced by a PSF shaped residual after the subtraction). As an alternative for subtracting the best fit for a star from the map the area within the PSF of a star can be replaced by the planar background obtained from the fit. This is guaranteed to remove the inherent noise in the bright star, at the expense of loosing information of variations in the background brightness on spatial scales of the PSF (of about one square degree). The result of this procedure is shown in the bottom two maps in Figure 4 for both least square fits. The difference between the two maps is minimal. For most of the heliospheric solar wind studies done with SMEI observations, involving large scale structures such as coronal mass ejections that usually cover many square degrees of sky, these subtracted maps are probably sufficient.

ACKNOWLEDGMENTS

This work was supported by NASA Grants NAG5-11906 and NAG5-134543; and USAF grant AF49620-01-1-0054. SMEI was designed and constructed by a team of scientists and engineers from the U.S. Air Force Research Laboratory, the University of California at San Diego, Boston College, Boston University, and the University of Birmingham in the U.K. Financial support was provided by the Air Force, the University of Birmingham, and NASA. The authors gratefully acknowledge the help of UCSD students Aaron Smith and John Clover.

REFERENCES

1. Buffington, A., Morrill, J.S., Hick, P.P, Howard, R.A. Jackson, B.V. and Webb, D.F., "Analysis of the comparative responses of SMEI and LASCO", *Proc. SPIE* **6689**, this meeting.
2. Eyles, C.J., Simnett, G.M., Cooke, M.P., Jackson, B.V., Buffington, A., Hick, P.P., Waltham, N.R., King, J.M., Anderson, P.A., and Holladay, P.E., "The Solar Mass Ejection Imager (SMEI)", *Solar Phys.* **217**, 319-347, 2003.
3. Jackson, B.V., Buffington, A., Hick, P.P., Altrock, R.C., Figueroa, S., Holladay, P.E., Johnston, J.C., Kahler, S.W., Mozer, J.B., Price, S., Radick, R.R., Sagalyn, R., Sinclair, D., Simnett, G.M., Eyles, C.J., Cooke, M.P., Tappin, S.J., Kuchar, T., Mizuno, D., Webb, D.F., Anderson, P.A., Keil, S.L., Gold, R.E., and Waltham, N.R., "The Solar Mass Ejection Imager (SMEI) mission" , *Solar Phys.* **225**, 177-207, 2004.
4. Buffington, A., Jackson, B.V., and Hick, P.P., "Am empirical description of zodiacal light as measured by SMEI", *EOS Trans. AGU* **87 (52)**, Fall Meet. Suppl., Abstract SH32A-06, 2006.
5. Mizuno, D.R., Buffington, A., Cooke, M.P., Eyles, C.J., Hick, P.P., Holladay, P.E., Jackson, B.V., Johnston, J.C., Kuchar, T.A., Mozer, J.M., Price, S.D., Radick, R.R., Simnett, G.M., Sinclair, D., Tappin, S.J., and Webb, D.F., "Very High Altitude Aurora Observations with the Solar Mass Ejection Imager", *J. Geophys. Res.* **110**, 7230-7247, 2005.
6. Hick, P.P., Buffington, A. and Jackson, B.V., "The SMEI real-time data pipeline: from raw CCD frames to photometrically accurate full-sky maps", *Proc. SPIE* **5901B**, 1-7, 2005.
7. Buffington, A., Jackson, B.V. and Hick, P.P., "Space performance of the multistage labyrinthine SMEI baffle", *Proc. SPIE* **5901**, 590118, 1-10, 2005.

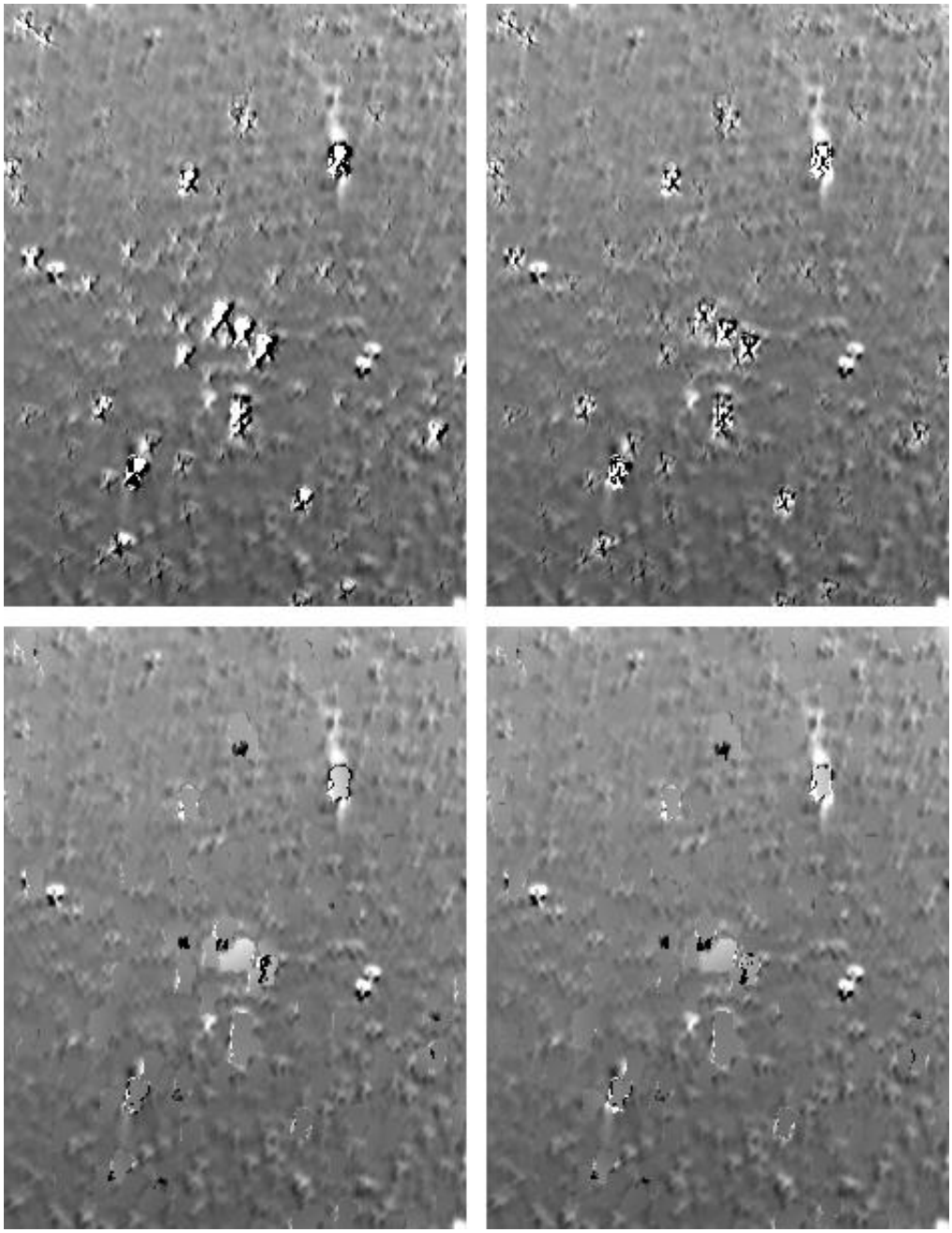

Figure 4. Results of star subtraction in Orion. 149 stars brighter than 6^{th} magnitude from the SMEI catalogue are subtracted. Top-left: subtraction of simple least square fit (Sections 3 and 4) solution. Top-right: subtraction of least squares fit with iterative solutions for centroid, PSF width and PSF orientation (Section 5). Bottom-left: same as top-left, but instead of subtracting the full least squares solution, the PSF is replaced by the planar background solution. Bottom-right: same as top-right, with the PSF replaced by the planar background solution. The grey scale covers the range 0 (black) to 100 ADUs (white); the average remaining background is about 50 ADUs.